Finite-Resolution Effects in p-Leader Multifractal Analysis

Roberto Leonarduzzi, *Member, IEEE*, Herwig Wendt, *Member, IEEE*, Patrice Abry, *Fellow, IEEE*, Stéphane Jaffard, and Clothilde Melot

***Abstract*—Multifractal analysis has become a standard signal processing tool, for which a promising new formulation, the p-leader multifractal formalism, has recently been proposed. It relies on novel multiscale quantities, the p-leaders, defined as local ℓ^p norms of sets of wavelet coefficients located at infinitely many fine scales. Computing such infinite sums from actual finite-resolution data requires truncations to the finest available scale, which results in biased p-leaders and thus in inaccurate estimates of multifractal properties. A systematic study of such finite-resolution effects leads to conjecture an explicit and universal closed-form correction that permits an accurate estimation of scaling exponents. This conjecture is formulated from the theoretical study of a particular class of models for multifractal processes, the wavelet-based cascades. The relevance and generality of the proposed conjecture is assessed by numerical simulations conducted over a large variety of multifractal processes. Finally, the relevance of the proposed corrected estimators is demonstrated on the analysis of heart rate variability data.**

***Index Terms*—Multifractal analysis, p-leaders, wavelet cascades.**

I. Introduction

A. Multifractal Analysis

MULTIFRACTAL analysis has become a standard signal processing tool, widely used and proven relevant in several different applications, including biomedicine [1], [2], finance [3], geophysics [4], [5], and art investigation [6], among many others. It amounts to estimating the so-called *multifractal spectrum* $D(h)$ of a signal or field X. $D(h)$ quantifies globally and geometrically the local variations of the *regularity* of X, measured by the *regularity exponent* h.

This work was supported by Grant ANR-16-CE33-0020 MultiFracs. (*Corresponding author: Roberto Leonarduzzi*.)

R. Leonarduzzi and P. Abry are with the Univ Lyon, Ens de Lyon, Univ Claude Bernard, CNRS, Laboratoire de Physique, F-69342, Lyon, France (e-mail: roberto.leonarduzzi@ens-lyon.fr; patrice.abry@ens-lyon.fr).

H. Wendt is with IRIT, CNRS UMR 5505, University of Toulouse, Toulouse 321000, France (e-mail: herwig.wendt@irit.fr).

S. Jaffard is with Université Paris Est, Laboratoire d'Analyse et de Mathématiques Appliquées, CNRS UMR 8050, UPEC, Créteil 94010, France (e-mail: jaffard@u-pec.fr).

C. Melot is with the Aix Marseille University, CNRS, Centrale Marseille, I2M, Marseille 13331, France (e-mail: clothilde.melot@univ-amu.fr).

Color versions of one or more of the figures in this paper are available online at http://ieeexplore.ieee.org.

Digital Object Identifier 10.1109/TSP.2017.2690391

B. Local Regularity

Traditional formulations of multifractal analysis rely on the use of the *Hölder exponent* as a measure of local regularity [7]–[9]. However, it has recently been proposed that multifractal analysis could be based on p-*exponents* instead [10], [11]. This new formulation presents three key advantages: i) it can be applied to a larger class of functions or signals X (functions that are locally in $L^p(\mathbb{R}^d)$ instead of locally bounded); ii) the variability of the fluctuations of local regularity with p provides additional information on the nature of singularities [12], [13]; iii) practical estimation methods yield estimates with significantly smaller variance [11].

C. Multifractal Formalism

Estimation of the multifractal spectrum is conducted in practice following the so-called *multifractal formalism* [7], [11], [14]. It provides an upper bound for $D(h)$ by analyzing the scaling behavior *in the limit of fine scales* of appropriate multiscale quantities, i.e., quantities with a joint time-scale localization. Estimates of the corresponding scaling exponents, and thus of $D(h)$, are obtained as linear regressions, over a large range of scales, of time-space averages of these quantities.

D. p-Leaders

It has been shown in [10], [11] that, when using p-exponents, the multifractal formalism must be based on special multiscale quantities: the so-called p-*leaders*. These quantities consist, at a given scale, of local weighted ℓ^p norms of wavelet coefficients, computed over narrow time neighbourhoods and *over all finer scales*. The p-*leader* multifractal formalism expands and enrich the earlier formulation relying on ℓ^∞ norms of wavelet coefficients, the *wavelet leaders* [7], [14], [15].

E. Finite-Resolution Effect

When computed from real-world finite-resolution data, p-leaders suffer from two distinct finite-resolution effects. The first issue is related to the fact that wavelet coefficients are theoretically defined as continuous-time inner products, which in practice must be approximated in discrete time. This subject has already been extensively addressed and shown to have a limited and well-documented impact on the estimation of scaling exponents, cf. e.g., [16], [17]. The second issue has a much more dramatic impact on estimation quality, and is related to the fact that p-leaders, for a given scale, are theoretically defined as sums *over all the infinitely many finer scales*. In practice the number

of scales is finite, and these sums must necessarily be truncated, yielding a systematic bias in the actually computed p-leaders. Even worse, this bias is more prominent at fine scales, which are predominantly involved in multifractal analysis, thus significantly impairing the estimation of multifractal parameters.

F. Goals, Contributions and Outline

The present contribution describes a thorough analysis of finite-resolution effects on p-leader-based multifractal analysis, and proposes a conjecture to practically correct for such effects. After a short review of the main elements of p-leader multifractal analysis in Section II, a conjecture permitting to correct for finite-resolution effects is proposed in Section III. It is then shown theoretically, in Section IV, that the proposed conjecture is exact for a special class of multifractal processes, the wavelet-based cascades. In Section V, the proposed conjecture is further validated by means of numerical simulations on several multifractal processes of different natures; p-leader estimation performance is also discussed. Finally, Section VI illustrates the relevance of correcting for finite-resolution effects on real data.

II. Multifractal Analysis and p-Leaders

A. p-Exponents and Multifractal Spectrum

The signal or field to be analyzed is hereafter denoted as $X : \mathbb{R}^d \to \mathbb{R}$. Let $X \in L^p_{loc}(\mathbb{R}^d)$ for $p \geq 1$. X belongs to $T^p_\alpha(x)$, with $\alpha > -d/p$, if there exist $C, R > 0$ and a polynomial P_x of degree less than α, such that $\forall a < R$, $\left(\frac{1}{a^d}\int_{B(x,a)} |X(u) - P_x(u)|du\right)^{1/p} \leq Ca^\alpha$, where $B(x,a)$ is the ball of radius a centered at x. The *p-exponent* of X at x is defined as $h_p(x) = \sup\{\alpha \,:\, X \in T^p_\alpha(x)\}$ [10], [18]. When $p = \infty$, the p-exponent $h_\infty(x)$ coincides with the traditional Hölder exponent $h(x)$ [7], [10], [19]. It measures the regularity of X at x: the smaller $h_p(x)$ is, the rougher and more irregular X is at x. Unlike the Hölder exponent, p-exponents allow to measure *negative regularity*, on condition though that $h_p(x) > -d/p$ [10].

Multifractal processes are usually defined by the fact that local regularity changes abruptly from one location to another, and a pointwise estimation of $h_p(x)$ is therefore of little interest, being itself a highly irregular function. Rather, one is interested in a function that quantifies globally the geometrical distribution of the values $h_p(x)$ takes on: the multifractal spectrum $D^{(p)}(h) = \dim_H\big(\{x \in \mathbb{R}^d \,:\, h_p(x) = h\}\big)$, where $\dim_H$ denotes the Hausdorff dimension. A practical estimate of $D^{(p)}(h)$ requires the use of multiscale quantities, which we now recall.

B. Wavelet p-Leaders

Let $\{\psi^{(i)}(x)\}_{i=1,\dots,2^d-1}$ denote a family of *mother wavelets*. These oscillating functions are characterized by a fast decay, good joint time-frequency localization, and guarantee a *number of vanishing moments* $N_\psi \in \mathbb{N}$, meaning that $\int x^k \psi^{(i)}(x)dx = 0$ for $k = 0, 1, \cdots, N_\psi - 1$. The collection $\{\psi^{(i)}(2^j x - k),\ i = 1, \cdots, 2^d - 1, j \in \mathbb{Z}, k \in \mathbb{Z}^d\}$ of dilated and translated versions of $\psi^{(i)}$ is an orthonormal basis of $L^2(\mathbb{R}^d)$. The discrete wavelet coefficients of X are then defined as: $e^{(i)}_{j,k} = 2^{dj}\int_{\mathbb{R}^d} X(x)\psi^{(i)}(2^j x - k)dx$. For more details on wavelet transforms, see, e.g., [20]. An L^1 normalization is used in this definition of wavelet coefficients since it is better suited for multifractal analysis.

For simplicity, let $k = (k_1, \dots, k_d) \in \mathbb{Z}^d$ and $\lambda = \lambda_{j,k} = \big[2^{-j}k_1, 2^{-j}(k_1+1)\big) \times \cdots \times \big[2^{-j}k_d, 2^{-j}(k_d+1)\big)$ label *dyadic cubes*. Each wavelet coefficient can be associated with one dyadic cube: $e^{(i)}_\lambda = e^{(i)}_{j,k}$. Let $\lambda(x)$ denote the only cube at scale j that includes x, and $3\lambda = 3\lambda_{j,k} = \big[2^{-j}(k_1 - 1), 2^{-j}(k_1+2)\big) \times \cdots \times \big[2^{-j}(k_d - 1), 2^{-j}(k_d+2)\big)$ denote the union of λ and its $3^d - 1$ neighbours.

Let $p > 0$ and $X \in L^p_{loc}(\mathbb{R}^d)$. The *wavelet p-leaders* are defined as [10], [11], [19]

$$\ell^{(p)}_{j,k} = \ell^{(p)}_{\lambda_{j,k}} := \left(\sum_{\substack{\lambda'_{j',k'} \subset 3\lambda_{j,k} \\ j \leq j' < \infty}} \sum_{i=1}^{2^d-1} \left|e^{(i)}_{\lambda'_{j',k'}}\right|^p 2^{d(j-j')}\right)^{\frac{1}{p}} \quad (1)$$

where $j' \geq j$ is the scale associated with the sub-cube λ'. Note that the outer sum is performed over all finer scales $j' \geq j$ and over a narrow spatial neighborhood of $x = 2^{-j}k$.

The key property of p-leaders is that their decay exactly reproduces the p-exponent: $\ell^{(p)}_{\lambda(x)} \sim 2^{-jh_p(x)}$ when $j \to \infty$ [7], [10], [11], [19].

When $p = \infty$, (1) reduces to the definition of wavelet leaders, as proposed in [14], [15].

C. Multifractal Formalism

The *multifractal formalism* permits to estimate $D^{(p)}(h)$ in a practically feasible and robust way. It is based on the so-called *structure functions*:

$$S_{\ell^{(p)}}(q, j) := \frac{1}{n_j}\sum_k \left|\ell^{(p)}_{j,k}\right|^q, \quad (2)$$

where n_j is the number of coefficients $\ell^{(p)}_\lambda$ available at scale j. For multifractal models, $S_{\ell^{(p)}}(q, j)$ exhibits a power-law decay, at fine scales, controlled by the *scaling exponent* $\zeta_{\ell^{(p)}}$:

$$S_{\ell^{(p)}}(q, j) \sim K_{p,q} 2^{-j\zeta_{\ell^{(p)}}(q)}, \quad j \to \infty. \quad (3)$$

A concave upper-bound for $D^{(p)}$, known as the *Legendre spectrum* $\mathcal{L}_{\ell^{(p)}}$, is provided by the Legendre transform of $\zeta_{\ell^{(p)}}$:

$$\mathcal{L}_{\ell^{(p)}}(h) := \inf_{q \in \mathbb{R}}\big(d + qh - \zeta_{\ell^{(p)}}(q)\big) \geq D^{(p)}(h), \quad (4)$$

with equality for numerous multifractal processes, and in particular for the ones used here, cf. [10]–[13].

D. Log-Cumulants

Log-cumulants summarize into a few parameters most of the relevant information contained in $\mathcal{L}_{\ell^{(p)}}$. They are defined as the coefficients of the Taylor expansion of the scaling function: $\zeta_{\ell^{(p)}}(q) := \sum_{m \geq 1} c_{\ell^{(p)}}(m) q^m / m!$. Use of the Legendre transform also provides an expansion of the $\mathcal{L}_{\ell^{(p)}}$ around its maximum (cf. [11], [15]), further permitting to interpret the $c_{\ell^{(p)}}(m)$: $c_{\ell^{(p)}}(1)$ is the location of the maximum of $\mathcal{L}_{\ell^{(p)}}$, $c_{\ell^{(p)}}(2)$ is related to its width, $c_{\ell^{(p)}}(3)$ is related to its asymmetry, etc. By

extending calculations in [11], [14], [21], it is straightforward to show that the $c_{\ell^{(p)}}(m)$ can be computed directly from the m-th order cumulants $C_{\ell^{(p)}}(m,j)$ of $\log \ell^{(p)}_{j,\cdot}$:

$$C_{\ell^{(p)}}(m,j) = C_{\ell^{(p)},0} + c_{\ell^{(p)}}(m)\log(2^{-j}) \quad j \to \infty. \tag{5}$$

E. Practical Estimates

In practice, $\zeta_{\ell^{(p)}}(q)$ and $c_{\ell^{(p)}}(m)$ are computed by linear regressions, as $\zeta_{\ell^{(p)}}(q) = \sum_{j=j_1}^{j_2} \omega_j \log_2 S_{\ell^{(p)}}(q,j)$ and $c_{\ell^{(p)}}(m) = \log_2(e)\sum_{j=j_1}^{j_2} b_j C_{\ell^{(p)}}(m,j)$, for scales j within the *scaling range* $[j_1, j_2]$, with classical linear regressions weigths b_j, cf. e.g., [15].

F. Minimum Regularity Hypothesis

Both p-exponents and p-leaders are defined only for functions $X \in L^p_{loc}(\mathbb{R}^d)$. It can be easily checked whether data practically satisfy such a property by an *a priori* analysis of the decay of their *wavelet structure function*

$$S_e(q,j) := \frac{1}{n_j}\sum_k \sum_{i=1}^{2^d-1} \left|e^{(i)}_{j,k}\right|^q, \quad q \geq 0. \tag{6}$$

Let $\eta(p)$ denote the *wavelet scaling function*

$$S_e(p,j) \sim K_p 2^{-j\eta(p)}, \quad j \to \infty. \tag{7}$$

It has been shown in [10] that if $\eta(p) > 0$, then $X \in L^p_{loc}(\mathbb{R}^d)$. It is useful to consider the *critical Lebesgue index* $p_0 = \sup(p : \eta(p) > 0)$: p-leaders are defined for $p < p_0$, and when this condition is not met, p-leader-based quantities are not defined theoretically and their practical estimation is thus meaningless [10], [11].

III. Finite-Resolution Effects and Estimation

A. Finite-Resolution Scaling Behavior

Equation (1) shows that the computation of $\ell^{(p)}_{j,k}$ at scale j requires the availability of wavelet coefficients across infinitely many finer scales j' such that $j \leq j' < \infty$. However, in practice, only a finite-size finite-resolution sampled version of the input data X is available. Therefore, wavelet coefficients can only be computed for a finite range of scales $\underline{j} \leq j \leq \bar{j}$, with $\underline{j}$ and $\bar{j}$ the coarsest and finest scales available. Thus, the outer sum in (1) can only be computed for the *finite* subset of scales $j \leq j' \leq \bar{j}$, giving rise to *finite-resolution p-leaders* $\breve{\ell}^{(p)}_\lambda$, which suffer from a systematic (under-estimation) bias.

B. Finite-Resolution Estimates

Let $S_{\breve{\ell}^{(p)}}(q,j)$ denote the structure functions computed from finite-resolution p-leaders $\breve{\ell}^{(p)}$. Motivated by preliminary analyses in [11] and analytical calculations of wavelet cascades detailed in Section IV, we define the following corrected estimate $\hat{S}_{\breve{\ell}^{(p)}}(q,j)$:

$$\hat{S}_{\breve{\ell}^{(p)}}(q,j) := S_{\breve{\ell}^{(p)}}(q,j)\,\gamma^{-\frac{q}{p}}(j,\eta(p)), \tag{8}$$

$$\text{with } \gamma(j,\eta(p)) = \left(\frac{1-2^{-(\bar{j}-j+1)\eta(p)}}{1-2^{-\eta(p)}}\right). \tag{9}$$

We conjecture that the corrected estimate $\hat{S}_{\breve{\ell}^{(p)}}(q,j)$ allows to recover the one which would be obtained from p-leaders computed from infinite-resolution data, i.e.,

$$\hat{S}_{\breve{\ell}^{(p)}}(q,j) \equiv S_{\ell^{(p)}}(q,j). \tag{10}$$

Equation (8) indicates that scaling in structure functions $S_{\breve{\ell}^{(p)}}$ computed from finite-resolution p-leaders is corrupted by the nonlinear term γ, whose form is conjectured in (9), which can be easily estimated and corrected for.

The following proposition extends Correction (8) to cumulants. The proof is sketched in Appendix A.

Proposition 1: If and only if (8) holds, the corrected cumulants $\hat{C}_{\breve{\ell}^{(p)}}(m,j)$ relate to finite- and infinite-resolution cumulants, $C_{\breve{\ell}^{(p)}}(m,j)$ and $C_{\ell^{(p)}}(m,j)$ respectively, as

$$\hat{C}_{\breve{\ell}^{(p)}}(1,j) = C_{\breve{\ell}^{(p)}}(1,j) - \frac{1}{p}\log\gamma(j,\eta(p)), \tag{11}$$

$$\hat{C}_{\breve{\ell}^{(p)}}(m,j) = C_{\breve{\ell}^{(p)}}(m,j) \qquad \text{for } m \geq 2, \tag{12}$$

$$C_{\ell^{(p)}}(m,j) \equiv \hat{C}_{\breve{\ell}^{(p)}}(m,j) \quad \forall m \in \mathbb{N}^+. \tag{13}$$

Remark 1: The fact that only the scaling of $C_{\breve{\ell}^{(p)}}(1,j)$ is corrupted by finite-resolution effects, while $C_{\breve{\ell}^{(p)}}(m,j)$ for $m \geq 2$ are not, implies that only the mode $c_{\ell^{(p)}}(1)$ of $\mathcal{L}_{\ell^{(p)}}$ (i.e., the average regularity) is biased, while the shape (width, asymmetry, ...) is not. Parameters $c_{\breve{\ell}^{(p)}}(m)$ for $m \geq 2$, are thus unaffected by finite-resolution effects and benefit from better estimation performance of p-leaders, as detailed in Section V-D and also reported in [11], without the need of correcting for finite-resolution effects.

Remark 2: Because $\gamma(j,\eta(p))$ decays exponentially at coarse scales, $j \to -\infty$, the finite-resolution effects become negligible at coarse scales, all the more when $\eta(p)$ is large.

Remark 3: When $p \to \infty$, the proposed correction terms in (8) and (11) vanish. Therefore, the conjectured perturbation of scaling at fine scales is not observed for traditional wavelet leaders (cf. Sections IV and V for details).

The following sections show the validity of the proposed corrected estimates, either theoretically in Section IV by analysis of a special class of multifractal processes, the wavelet cascades, or empirically in Section V by means of numerical simulations conducted over several multifractal processes different in nature.

IV. Theoretical Results

In this section, finite-resolution effects are investigated theoretically on functions defined directly by wavelet coefficients, i.e., 1D and 2D deterministic or random wavelet cascades, for which S_e and C_e can be regarded as the exact scaling quantities.

For ease of exposition, this section makes use of the *restricted p-leaders* $\ell^{(p)}_\lambda$, defined by replacing 3λ with λ in (1): $\ell^{(p)}_{j,k} = \ell^{(p)}_\lambda = \left(\sum_{\lambda'\subset\lambda}\sum_{i=1}^{2^d-1}|c^{(i)}_{\lambda'}|^p 2^{d(j-j')}\right)^{1/p}$. It has been

shown that structure functions computed with restricted p-leaders and p-leaders as in (1) are equivalent (cf. [22]).

A. Deterministic Binomial Wavelet Cascade

1) Construction: Inspired by [23], we propose a model for 2D Deterministic Binomial Wavelet Cascade (DBWC), whose wavelet coefficients are defined as follows:

$$\begin{cases} d_{0,1,1} & = 1 \\ d_{j,2k_1,2k_2} & = w_0\, d_{j-1,k_1,k_2} \\ d_{j,2k_1+1,2k_2} & = w_1\, d_{j-1,k_1,k_2} \\ d_{j,2k_1,2k_2+1} & = w_2\, d_{j-1,k_1,k_2} \\ d_{j,2k_1+1,2k_2+1} & = w_3\, d_{j-1,k_1,k_2} \\ e^{(i)}_{j,k_1,k_2} & = \alpha_i\, d_{j,k_1,k_2} \end{cases} \tag{14}$$

with weights w_i being deterministic constants controlling multifractal properties, and $\alpha = (\alpha_i)$ controlling anisotropy. It can be shown that the wavelet scaling function η reads (cf. Appendix B),

$$\eta(q) = 2 - \log_2 \sum_{m=0}^{3} w_m^q\,, \quad \text{for } q > 0 \tag{15}$$

and that DBWC satisfies $\zeta_{\ell^{(p)}}(q) = \eta(q)$, $q > 0$, while anisotropy has no impact on the scaling properties.

2) p-Leader Analysis: Finite-resolution effects for 2D DBWC are described by the following proposition.

Proposition 2: The finite-resolution p-leader structure functions of a 2D DBWC as in (14) are given by

$$S_{\check{\ell}^{(p)}}(q,j) = \|\alpha\|_p\; S_e(q,j)\; \gamma^{\frac{q}{p}}\left(j,\eta(p)\right), \tag{16}$$

where the function γ is defined in (9).

The proof, cf. Appendix C, relies on the multiplicative structure of wavelet coefficients. Comparing (16) with (8) shows the relevance of the proposed correction. Similar computations for 1D DBWC lead to identical conclusions, with notably the same correction function γ (cf. [11]).

B. Multiplicative Random Wavelet Series (MRWS)

1) Construction: Random wavelet series (RWS), originally introduced in [24], are a general framework for constructing multifractal functions from their wavelet expansion. They are built by assigning to each wavelet coefficient an independent realization of a random variable. Here, we will consider the specific case of multiplicative RWS. Let $\{W\}^{(j)}$ denote the product of j independent copies of the continuous positive random variable W. Let $e_{0,1} = 1$. Then, the 2^j coefficients at scale $j > 0$ are built as $e_{j,k} \overset{\mathcal{L}}{=} \{W\}^{(j)}$. The wavelet scaling function η, for $q > 0$, reads $\eta(q) = -\log_2 \mathbb{E}[W^q]$ under suitable assumptions on the tail of W [25], and MRWS satisfy $\zeta_{\ell^{(p)}}(q) = \eta(q)$, for $q > 0$.

2) p-Leader Analysis: First, we analyze the behavior of $S_{\check{\ell}^{(p)}}(q,j)$ for q a multiple of p.

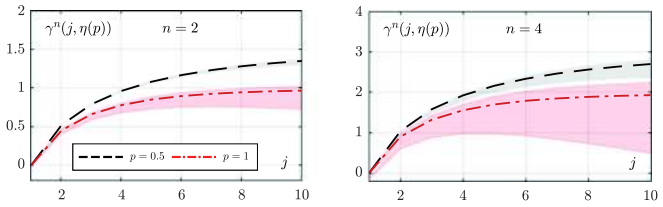

Fig. 1. MRWS structure functions. Proposed correction $\gamma^n\,(j,\eta(p))$, for two values of n (left and right panels), and $p = 0.5$ (black dashed line) and $p = 1$ (red dash-dotted line). The solid lines that delimit the shaded areas represent the bounds $b_S\,(n,p,j)$ and $B_S\,(n,p,j)$, which converge to each other for small j and p.

Proposition 3: Let $q = np$, $n \in \mathbb{N}$. The MRWS finite-resolution p-leader structure function $S_{\check{\ell}^{(p)}}(q,j)$ satisfies:

$$b_S\,(n,p,j) \le \frac{S_{\check{\ell}^{(p)}}(q,j)}{S_e(q,j)\,\gamma^n\,(j,\eta(p))} \le B_S\,(n,p,j)\,, \tag{17}$$

with

$$b_S\,(n,p,j) = 2^{-j(n\eta(p)-\eta(np))}, \tag{18}$$

$$B_S\,(n,p,j) = \frac{\gamma^n\,(j,\eta(np)/n)}{\gamma^n\,(j,\eta(p))}, \tag{19}$$

and where the function γ is defined in (9).

The proof, cf. Appendix D, relies on the multiplicative structure of wavelet coefficients and the concavity of the scaling function. Proposition 3 can be extended to all positive values of q, as in the following consequence.

Consequence 1: Assuming that $S_{\check{\ell}^{(p)}}(np,j)$ and $S_e(np,j)$ are smooth enough as functions of n, then Prop. 3 also holds for $n \in \mathbb{R}^+$.

The proof, cf. Appendix E, is based on an interpolation argument.

3) Remarks: Proposition 3 shows that, for MRWS, we are only able to produce bounds for the deviation from exact scaling induced by finite-resolution effects. However, the bounds b_S and B_S tend to coincide for small values of p, $q = np$ and j, as illustrated in Fig. 1. Thus, the proposed corrections can be assumed to be asymptotically exact in those situations when the finite-resolution effects are the strongest (small p and fine scales $j \to \bar{j}$). Also, the lower and upper bounds coincide when η is a linear function, indicating that the proposed corrections are exact for monofractal MRWS.

C. Random Wavelet Cascades (RWC)

1) Construction: The MRWS analyzed in the previous section have independent wavelet coefficients. We now consider a related process with strongly correlated wavelet coefficients: the random wavelet cascades (RWC) [25]. Let $e_{j,k} = 1$, and let W_l, W_r and W denote iid positive random variables. Wavelet coefficients at scales $j = 1, 2, \cdots, \bar{j}$ are built from coefficients at scale $j-1$ by the iterative procedure $e_{j,2k} = W_l e_{j-1,k}$, $e_{j,2k+1} = W_r e_{j-1,k}$. The wavelet scaling function η, defined for $q > 0$, is also shown to read $\eta(q) = -\log_2 \mathbb{E}[W^q]$ under suitable assumptions on the tail of W [25], and RWC satisfies $\zeta_{\ell^{(p)}}(q) = \eta(q)$ for $q > 0$.

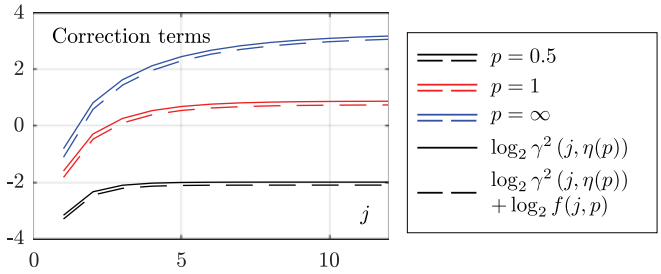

Fig. 2. Random wavelet cascades, $q = 2p$. Correction terms $\log_2 \gamma^2(j, \eta(p))$ (solid) and $\log_2 \gamma^2(j, \eta(p))\, f(j, p)$ (dashed), for several values of p (colors). The difference is negligible.

2) p-Leader Analysis: The complicated correlation structure precludes the computation of the structure functions for an arbitrary q. Thus, we restrict calculations to $q = p$ and $q = 2p$.

Proposition 4: For $q = p$, the p-leader structure function of a RWC reads

$$S_{\check{\ell}(p)}(p, j) = S_e(p, j)\, \gamma(j, \eta(p)) \tag{20}$$

where the function γ is defined in (9).

Proposition 5: For $q = 2p$, the p-leader structure function of a RWC reads

$$S_{\check{\ell}(p)}(2p, j) = S_e(2p, j) \gamma^2(j, \eta(p))\; f(j, p), \tag{21}$$

where

$$f(j, p) = \frac{1}{2 - 2^{-\mu(p)+1}} \left[1 - 2^{\mu(p)} \frac{\gamma(j, \mu(p))}{\gamma(j, \eta(p))}\right], \tag{22}$$

with $\mu(p) = \eta(2p) - \eta(p) + 1$, and γ is defined in (9).

Proofs are given in Appendix F. Proposition 5 shows that, in the presence of correlations, the finite-resolution effect theoretically differs from the correction conjectured in (8) by the higher-order term $f(j, p)$. However, extensive numerical simulations indicate that this term has negligible effect. This is illustrated in Fig. 2, using $\eta(p) = c(1)p + c(2)^2/2$, a typical example for many processes (here with $c(1) = 0.8$ and $c(2) = -0.08$).

V. Empirical Assessment

A. Multifractal Processes

In this section, we investigate the level of validity of the proposed corrected estimates of Section III-B in a general setting, using a representative panel of multifractal processes.

1) Fractional Brownian Motion (fBm): fBm is defined as the integral of a Gaussian noise with a kernel that defines its covariance structure [26], [27], fully controlled by the *Hurst parameter* H. fBm is monofractal, which means that its $D^{(p)}$ collapses to a single point.

2) Multifractal Random Walk (MRW): MRW is defined from two independent Gaussian processes, with a specific covariance structure chosen to mimic that of multiplicative cascades [28]. A 2D extension has been proposed in [29]. It has a parabolic $D^{(p)}$ controlled by two parameters, H and λ. Expressions for its multifractal spectrum and p_0 are provided in [11], [28], [29].

3) α-Stable Lévy Process: An α-stable Lévy process is defined as a selfsimilar process with independent stationary increments [27]. It has a linear $D^{(p)}$, controlled by the selfsimilarity exponent α. Expressions for the multifractal spectrum and p_0 are given in [30], [31].

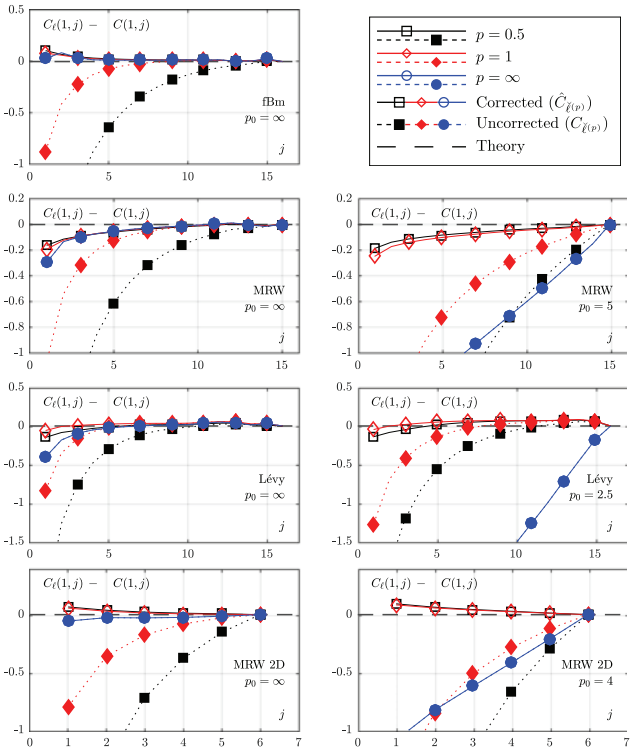

Fig. 3. Logscale diagrams: impact of correction. Logscale diagrams for different processes (rows) and values of p_0 (columns). Solid lines with empty markers represent corrected $\hat{C}_{\check{\ell}(p)}(1, j)$, while dashed lines with solid markers represent uncorrected $C_{\check{\ell}(p)}(1, j)$. Marker-styles and colors indicate different values of p.

a) Critical Lebesgue index: The critical Lebesgue index p_0 is always ∞ for the considered processes. For MRW and α-stable Lévy process, we will also analyze their fractional derivatives, which have a finite p_0 tuned by the differentiation order (cf. [11], [31]).

B. Simulation Setup

$N_{MC} = 100$ realizations of each multifractal process are analyzed, of size $N = 2^{19}$ for 1D processes and $N_1 \times N_2 = 2^{10} \times 2^{10}$ for 2D processes. In all cases, averages over the N_{MC} realizations are reported. The synthesis parameters were set to $H = 0.7$ for fBm, $H = 0.84$ and $\lambda = \sqrt{0.08}$ for MRW (both 1D and 2D), and $\alpha = 0.8$ for Lévy process.

Wavelet analysis is performed using a Daubechies wavelet with $N_\psi = 3$ vanishing moments. p-leaders are computed for $p \in \{1/4, 1/2, 1, 2, 5, \infty\}$, and the convention that the finest available scale is $\bar{j} = 1$. Scaling exponents and log-cumulants are computed using weighted linear regressions [14].

C. Logscale Diagrams

1) Impact of the Proposed Correction for $C(1, j)$: We begin by analyzing qualitatively and quantitatively how the proposed correction enables to restore the correct scaling behavior for $C(1, j)$. Fig. 3 superimposes cumulants with correction $\hat{C}_{\check{\ell}(p)}(1, j) - C(1, j)$ (solid lines, empty markers) and without correction $C_{\check{\ell}(p)}(1, j) - C(1, j)$ (dotted lines, full markers), for

TABLE I
RELATIVE SQUARED ERROR IN DEPARTURES FROM SCALING

		p			
	p_0	0.5	1	2	5
fBm	∞	2.81	1.72	0.28	-0.03
MRW	1.3	2.39	1.76	1.25	1.51
	2.5	2.97	2.15	1.42	1.56
	5	2.71	1.82	0.99	0.61
	∞	2.35	1.29	0.46	0.05
Lévy	1.3	3.66	2.53	2.40	2.77
	2.5	3.09	1.85	0.80	1.54
	5	3.01	1.89	1.00	-0.13
	∞	2.71	1.62	1.30	0.93
MRW 2D	1.5	3.31	2.76	2.39	2.70
	2.8	2.74	2.13	1.6	1.41
	5.3	3.05	2.42	1.88	2.02
	∞	2.93	2.13	1.25	0.55

$\log_{10}(SE_{\ell(p)}/SE_{\check{\ell}(p)})$, where $SE_{\ell(p)}$ and $SE_{\check{\ell}(p)}$ are the squared errors quantified the departures of $\hat{C}_{\check{\ell}(p)}(1,j)$ and $C_{\check{\ell}(p)}(1,j)$ from the exact theoretical scaling.

several values of p and p_0. The subtraction of the true scaling $C(1,j)$ is intended to ease comparisons since departures from perfect estimation thus materialize as departures from 0. Fig. 3 strikingly shows that uncorrected $C_{\check{\ell}(p)}(1,j)$ present significant departures from the theoretical scaling, and clearly depart one from another for different values of p. To the contrary, corrected $\hat{C}_{\check{\ell}(p)}(1,j)$ show very mild departures from the theoretical scaling, and additionally they all coincide. These are very satisfactory outcomes as it is known theoretically that for all processes analyzed here the multifractal spectra $D^{(p)}(h)$ (and hence $C(1,j)$) do not depend on p. These observations suggest that the conjectured correction (11) is valid and effective for a much larger class of processes than those studied in Section IV. Uncorrected $C_{\check{\ell}(p)}(1,j)$ yield departures from theoretical behavior that are larger for small p as well as for $p_0<\infty$, which is consistent with the fact that $\eta(p)$ is smaller for small values of p and of p_0.

1) Remark: Despite the fact that wavelet leaders ($p=\infty$) are not defined for $p_0<\infty$ [10], they can still be computed in practice. However—as shown in Fig. 3(right)—these practical estimates are affected by a strong bias, which is explicitly accounted for in [11], [31].

2) Quantitative Assessment: To further assess the relevance of the correction on the logscale diagrams we propose to quantify the deviations from true scaling by the squared error $SE_{\ell(p)}=\langle\sum_{j=\bar{j}}^{j}(\hat{C}_{\check{\ell}(p)}(1,j)-C(1,j))^2\rangle_N$, where $\langle\cdot\rangle_N$ stands for the average over N independent realizations, and compare them to the deviations $SE_{\check{\ell}(p)}$ yielded when no correction is used, i.e., by $C_{\check{\ell}(p)}(1,j)$. Because only the scaling behavior is of interest here, the influence of the intersect $C^{(p,0)}(1)$ is removed, by simple substraction so that $C_{\ell(p)}(1,\underline{j})-C(1,\underline{j})=0$ (and similarly for $C_{\check{\ell}(p)}(1,j)$). Table I reports results in terms of $\log_{10}(SE_{\ell(p)}/SE_{\check{\ell}(p)})$ for several p_0 and p. The fact that most entries in Table I are positive confirms that the use of the correction lessens the difference with the correct scaling behavior. Notably, for small p and p_0, the corrected estimator $\hat{C}_{\check{\ell}(p)}(1,j)$ improves the squared error by 3 orders of magnitude over the uncorrected $C_{\check{\ell}(p)}(1,j)$. For larger p and p_0, where the impact of correction appears to be less significant, the scaling of $C_{\check{\ell}(p)}(1,j)$ is actually already close to the theoretical one; correction is thus less needed.

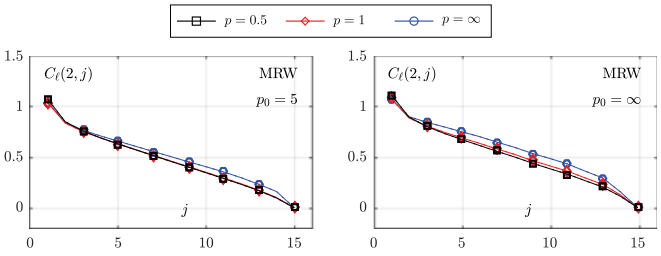

Fig. 4. Uncorrected logscale diagrams $C_{\check{\ell}(p)}(2,j)$, for MRW, for different values of p and p_0.

3) Logscale Diagrams for $C(m,j)$, $m\geq 2$: Fig. 4 provides examples of $C_{\check{\ell}(p)}(2,j)$ for MRW, for two different critical Lebesgue indices p_0, and different p s. Fig. 4 clearly shows that $\hat{C}_{\check{\ell}(p)}(2,j)$, for all p, reproduce the expected theoretical scaling, as functions of scales j, independently of p_0, and that, as expected, the $\hat{C}_{\check{\ell}(p)}(2,j)$ superimpose for all p. This confirms numerically that no finite-resolution effects are observed on the higher-order cumulants $C_{\check{\ell}(p)}(m,j)$, $m\geq 2$, and thus no correction is needed, cf. (12).

4) Structure Functions $S_{\check{\ell}(p)}(q,j)$ and $S_{\ell(p)}(q,j)$: Since the scaling of structure functions can be directly translated into the scaling of cumulants (cf., Section II-D and Proposition 1), the relevance of the correction for the structure function $S_{\ell(p)}(q,j)$ is directly determined by the relevance and accuracy of the correction for the first cumulant, $\hat{C}_{\check{\ell}(p)}(1,j)$, which has been extensively assessed above. Therefore, the above results and conclusions for $\hat{C}_{\check{\ell}(p)}(1,j)$ directly apply to structure functions, and are not reproduced or further discussed here.

Overall, these results unambiguously indicate that the conjectured corrections (8-9) generically and robustly enable to remove the finite-resolution bias from cumulants and structure functions, and to restore their expected scaling behavior.

D. Estimation Performance for Scaling Parameters

1) Estimation of $c(1)$: Estimation of scaling parameters requires the selection of a range of scales where the linear regression is performed. As suggested in Fig. 3, the impact of finite-resolution effects on the bias of scaling-parameter estimates could be reduced by performing linear regressions at sufficiently coarse scales, yet at the price of a significant increase of the corresponding estimation variance. To quantify this, we set the upper limit of the scaling range j_2 to the coarsest available scale, and evaluate estimation performance for linear regressions conducted from all possible lower limits j_1, with both corrected and uncorrected cumulants $\hat{C}_{\check{\ell}(p)}(1,j)$ and $C_{\check{\ell}(p)}(1,j)$.

Estimation performances for $c(1)$ as functions of j_1 are compared in Fig. 5, for MRW, in terms of bias, standard deviation (std) and root mean squared error (rmse). Benefits of the proposed correction on estimation performance are striking. First, bias is significantly reduced for $\hat{c}_{\check{\ell}(p)}(1)$ as compared to that of $c_{\check{\ell}(p)}(1)$, which is subject to a dramatic blow-up for small values of j_1. Second, correction for the bias does not alter the std. Consequently, the smallest rmse for $\hat{c}_{\check{\ell}(p)}(1)$ is achieved at $j_1=5$ while only at scale $j_1=7$ for $c_{\check{\ell}(p)}(1)$, i.e., the correction enables the *use of finer scales* in linear regression; moreover, the optimal $rmse$ is smaller for $\hat{c}_{\check{\ell}(p)}(1)$ than for $c_{\check{\ell}(p)}(1)$.

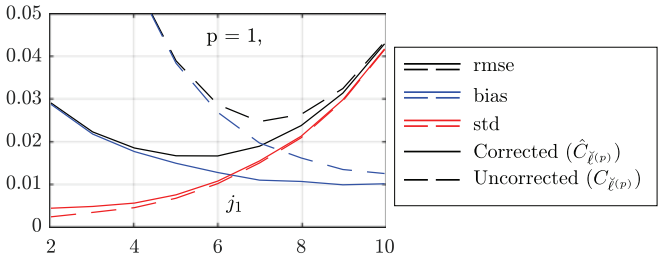

Fig. 5. Estimation performance (bias, std, rmse) for estimates $c_{\ell(p)}(1)$ and $\hat{c}_{\ell(p)}(1)$ as functions of lower scale j_1. Solid lines represent corrected $\hat{C}_{\ell(p)}(1,j)$, while dashed lines represent uncorrected $\hat{C}_{\ell(p)}(1,j)$. The upper scale j_2 was set to the largest available scale.

TABLE II
OPTIMAL RMSE AND LOWER CUTOFF

		$\log_{10}$(RORMSE)			OLC($c_{\ell(p)}(1)$) / OLC($\hat{c}_{\ell(p)}(1)$)		
		p			p		
	p_0	**0.5**	**2**	**5**	**0.5**	**2**	**5**
fBm	∞	0.98	−0.11	0.00	9 / 5	2 / 3	3 / 3
MRW	**1.3**	0.85	0.60	0.62	9 / 5	9 / 5	8 / 5
	2.5	0.81	0.52	0.50	9 / 6	9 / 6	8 / 5
	5	0.63	0.30	0.17	9 / 5	8 / 6	8 / 7
	∞	0.17	0.02	0.00	9 / 4	5 / 4	4 / 4
Lévy	**1.2**	0.59	0.81	0.83	9 / 3	7 / 1	5 / 1
	2.5	0.30	0.43	0.46	9 / 3	7 / 1	3 / 1
	5	0.19	0.13	−0.17	9 / 5	5 / 2	5 / 1
	∞	0.18	0.00	−0.51	9 / 4	3 / 2	3 / 1
MRW 2D	**1.5**	0.84	0.68	0.51	5 / 1	4 / 1	3 / 1
	2.8	0.76	0.59	0.42	5 / 1	4 / 1	3 / 1
	5.3	0.74	0.51	0.22	5 / 1	4 / 1	3 / 1
	∞	0.46	0.15	−0.17	5 / 2	3 / 2	1 / 1

Left panel: relative optimal rmse RORMSE; larger values indicate a larger gain due to the correction term. Right panel: optimal lower cutoffs $\mathrm{OLC}(c(1)) = \arg\min_{j_1} \mathrm{rmse}(j_1; c_1)$ for $c_{\ell(p)}(1)$ and $\hat{c}_{\ell(p)}(1)$.

To further quantify the decrease in rmse and in usable fine scales yielded by the conjectured correction, Table II (left panel) reports the relative optimal rmse (RORMSE) for $\hat{c}_{\ell(p)}(1)$ and $c_{\ell(p)}(1)$, defined as $\mathrm{RORMSE} = \min_{j_1} \mathrm{rmse}(j_1; c_{\ell(p)}(1)) / \min_{j_1} \mathrm{rmse}(j_1; \hat{c}_{\ell(p)}(1))$. Table II clearly demonstrates that using the correction (11) can yield considerable reductions of rmse values, by up to one order of magnitude. The gains in rmse are smaller for large p and p_0, as can be expected from the fact that in these cases $\eta(p)$ takes on large values and finite-resolution effects are hence negligible. In Table II (right panel), the choices of fine scale j_1 that lead to best rmse values, denoted optimal lower cutoff (OLC) and defined as $\mathrm{OLC}(c(1)) = \arg\min_{j_1} \mathrm{rmse}(j_1; c(1))$, are compared for $c_{\ell(p)}(1)$ and $\hat{c}_{\ell(p)}(1)$. The OLC values indicate that the conjectured correction indeed permits the use of several additional finer scales for scaling parameter estimation, thus explaining the origin in the reduction of RORMSE.

2) Estimation of c_m, $m \geq 2$: Table III reports the rmse for estimates $\hat{c}_{\ell(p)}(m)$, for $m = 1, 2, 3$, for MRW and different p and p_0, and shows that: i) the rmse for $\hat{c}_{\ell(p)}(m)$ always decreases with p; ii) while the rmse of $\hat{c}_{\ell(p)}(1)$ and $c_e(1)$ are similar, there is a large difference for $m \geq 2$, illustrating the inability of wavelet coefficients to estimate higher-order log-cumulants, and iii) while decreasing p_0 increases the rmse of $\hat{c}_{\ell(p)}(1)$ when $p > p_0$, it is not the case for higher-order log-cumulants (cf. [31] for details). These results clearly indicate that p-leader multifractal analysis with small p always yields the best estimation performance (see also [11]).

TABLE III
$\log_{10}(rmse)$ OF $\hat{c}_{\ell(p)}(m)$ AND $c_e(m)$ FOR MRW WITH DIFFERENT VALUES OF p_0 AND p

	p_0	$p = 0.5$	$p = 2$	$p = 5$	$p = \infty$	DWT
$c(1)$	1.3	−1.76	−1.61	−1.48	−0.513	−1.77
	2.5	−1.8	−1.66	−1.52	−0.593	−1.79
	5	−1.78	−1.65	−1.51	−0.807	−1.68
	∞	−1.79	−1.78	−1.76	−1.75	−1.69
$c(2)$	1.3	−2.16	−2.13	−2.04	−1.92	−1.37
	2.5	−2.16	−2.17	−2.07	−1.89	−1.35
	5	−2.16	−2.1	−2	−1.9	−1.33
	∞	−2.05	−1.9	−1.84	−1.85	−1.38
$c(3)$	1.3	−2.1	−2.09	−2.02	−1.83	−0.727
	2.5	−2.05	−1.96	−1.85	−1.74	−0.685
	5	−2.07	−2	−1.88	−1.78	−0.688
	∞	−1.88	−1.7	−1.65	−1.63	−0.625

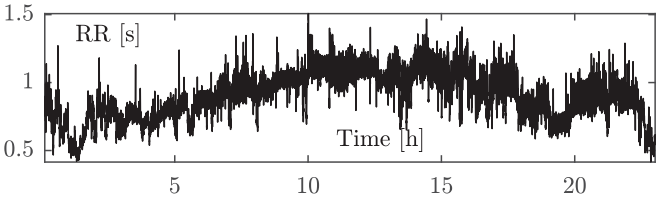

Fig. 6. Sample heart rate data. Record *nsr046* of the Normal Sinus Rhythm Physionet Database.

3) Importance of Accounting for Finite-Resolution Effects: This section demonstrated, first, that corrections (8) and (11) are robust and valid for large classes of processes and, second, that they permit a dramatic improvement in the accuracy of p-leader-based scaling analysis by: i) significantly reducing estimation bias, whatever j_1; ii) allowing to use several additional fine scales; iii) reducing rmse for the estimation of $c(1)$ by up to an order of magnitude.

VI. FINITE-RESOLUTION EFFECT IN HEART RATE DATA

Finally, the impacts of finite-resolution effects and the importance of using corrected p-leader scaling exponent analysis is illustrated on heart rate (HR) analysis of Normal Sinus Rhythm, made available by Physionet [32]. In this database, heart beats (RR intervals) were extracted by a standard automated procedure and revised by experts. Following standard practice, RR intervals were interpolated into a regularly sampled time series, using cubic splines, at $f_s = 4$ Hz.

The time series corresponding to record *nsr046* is shown in Fig. 6. The procedures described in Section II-F enable us to estimate $\hat{p}_0 = 7$. Fig. 7 reports the corrected $\hat{C}_{\ell(p)}(1,j)$ and uncorrected $C_{\ell(p)}(1,j)$ cumulants for $p = 0.25, 0.5$ and 1. Fig. 7 clearly shows that uncorrected estimates for all chosen p s are affected by finite-resolution effects. Conversely, corrected estimates $\hat{C}_{\ell(p)}(1,j)$ for all p collapse to a single function $C(1,j)$ which can hence be considered as the actual scaling behavior of these data. This example illustrates that the estimation of the position of the maximum of the multifractal spectrum, which has been shown to be a relevant feature to discriminate healthy from nonhealthy HR [33], is biased by finite-resolution effects, that can be well accounted for by the proposed systematic correction.

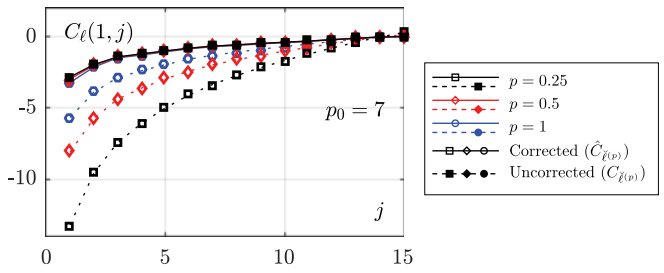

Fig. 7. Heart rate data: logscale diagrams. Solid lines represent corrected $\hat{C}_{\check{\ell}(p)}(1,j)$, while dashed lines with solid markers represent uncorrected $C_{\check{\ell}(p)}(1,j)$. Marker-styles and colors indicate different values of p. The $\hat{C}_{\check{\ell}(p)}(1,j)$ coincide for different p, as opposed to uncorrected $C_{\check{\ell}(p)}(1,j)$.

VII. Conclusion

This contribution reports a thorough analysis of the finite-resolution effect that arises when computing p-leaders from finite-resolution data. Explicit closed-form relations were derived to account for such finite-resolution effect, permitting to define corrected estimators than can be efficiently used in practice. The complicated nonlinear definition of p-leaders precluded their closed-form computation for general functions or random processes; in consequence, no general proof of the validity of the proposed corrections has been obtained so far —but is undergoing further investigation. Nonetheless, we assessed their effectiveness in two ways. First, a theoretical analysis of multifractal cascades enabled an explicit computation of p-leaders and showed the relevance of the proposed corrections for both 1D and 2D cascades, with very different correlation structures. Second, numerical simulations allowed to show that the proposed correction is valid for several types of multifractal processes of different natures. Further, it was shown that corrected p-leaders have better estimation performance than wavelet coefficients or state-of-the-art wavelet leaders. Finally, the relevance of these issues for real-life heart rate data was illustrated. The developments proposed in this work permit to make use of the theoretical and practical benefits of p-leaders for the multifractal analysis of data. A MATLAB toolbox for p-leader multifractal analysis is available at `http://www.irit.fr/%7EHerwig.Wendt/`.

Appendix

A. Proof of Proposition 1

We follow the derivation of the log-cumulants in [11], [14], [21]. For infinite-resolution p-leaders, assuming that the moments of order q exist and that $\mathbb{E}\left[(\ell_\lambda^{(p)})^q\right] = F_q 2^{-j\zeta_{\ell(p)}(q)}$, a standard generating function argument yields, for q close to 0, that

$$F_q 2^{-j\zeta_{\ell(p)}(q)} = \log \mathbb{E}\left[e^{q\ell_\lambda^{(p)}}\right] = \sum_{m\geq 1} C_{\ell(p)}(m,j)\frac{q^m}{m!}. \quad (23)$$

Now we consider finite-resolution p-leaders. Assuming (8) and (10), and that moments of order q exist, we can deduce that the expectation of p-leaders satisfies

$$\mathbb{E}\left[(\check{\ell}_\lambda^{(p)})^q\right]\gamma^{-\frac{q}{p}}(j,\eta(p)) = F_q 2^{-j\zeta_{\ell(p)}(q)}. \quad (24)$$

Then, for q close to 0 we have

$$F_q 2^{-j\zeta_{\ell(p)}(q)} = \log \mathbb{E}\left[e^{q\check{\ell}_\lambda^{(p)}}\right] - \frac{q}{p}\log\gamma(j,\eta(p)) \quad (25)$$

$$= \sum_{m\geq 1} C_{\check{\ell}(p)}(m,j)\frac{q^m}{m!} - \frac{q}{p}\log\gamma(j,\eta(p)) \quad (26)$$

$$= \sum_{m\geq 1} \hat{C}_{\check{\ell}(p)}(m,j)\frac{q^m}{m!}, \quad (27)$$

where

$$\hat{C}_{\check{\ell}(p)}(m,j) = \begin{cases} C_{\check{\ell}(p)}(m,j) - \frac{q}{p}\log\gamma(j,\eta(p)) & \text{if } m = 1 \\ C_{\check{\ell}(p)}(m,j) & \text{if } m \geq 2 \end{cases}, \quad (28)$$

which proves the direct statement. The proof of the converse statement is similar.

B. Proof of (15)

Coefficients d_{j,k_1,k_2} take on values of the form $w_0^{n_0}w_1^{n_1}w_2^{n_2}w_3^{n_3}$, with $n_0+n_1+n_2+n_3 = j$. Further, from the tree structure of the cascade we have that

$$\#\{d_{j,\cdot,\cdot} \,:\, n_0+n_1+n_2+n_3 = j\} = \binom{j}{n_0, n_1, n_2, n_3}.$$

Therefore, the wavelet structure function can be computed by application of the multinomial theorem:

$$S_e(q,j) = 2^{-2j}\sum_{k_1,k_2}\sum_i |e^{(i)}_{j,k_1,k_2}|^q$$

$$= \|\alpha\|_q^q \left(\frac{w_0^q + w_1^q + w_2^q + w_3^q}{4}\right)^j. \quad (29)$$

The wavelet scaling function η is defined by the scaling relation $S_c(q,j) \sim K 2^{-j\eta(q)}$. Therefore, we can define:

$$\eta(q) = 2 - \log_2 \sum_{m=0}^{3} w_m^q, \quad \text{for } q > 0. \quad (30)$$

C. Proof of Proposition 2

The structure of the cascade implies that, for a fixed point x and $j' > j$, $d_{\lambda'(x)} = d_{\lambda(x)} w_{m_1} w_{m_2} \cdots w_{m_{j'-j}}$, where the $m_i \in \{0,1,2,3\}$ take on values depending on each particular path on the subtree rooted in d_λ. Then, using (30) we can compute the restricted p-leaders as

$$\check{\ell}_\lambda^{(p)} = \left(\sum_{\lambda'\subset\lambda}\sum_i |e^{(i)}_{\lambda'}|^p 2^{-2(j'-j)}\right)^{1/p}$$

$$= \|\alpha\|_p d_\lambda \left(\sum_{l=0}^{\bar{j}-j} 2^{-2l}\sum_{k_1,k_2} d^p_{j+l,k_1,k_2}\right)^{1/p}$$

$$= \|\alpha\|_p d_\lambda \left(\sum_{l=0}^{\bar{j}-j} 2^{-l\eta(p)}\right)^{1/p}. \quad (31)$$

Using (2) and (31), we get:

$$S_{\breve{\ell}^{(p)}}(q,j) = \|\alpha\|_p \frac{1}{n_j} \sum_{k_1,k_2} d_\lambda^q \left(\sum_{l=0}^{\bar{j}-j} 2^{-l\eta(p)} \right)^{q/p}. \quad (32)$$

For finite-resolution $\bar{j} < \infty$, the geometric sum in (32) adds up to $\frac{1-2^{-(\bar{j}-j+1)\eta(p)}}{1-2^{-\eta(p)}}$ and hence the structure function is:

$$S_{\breve{\ell}^{(p)}}(q,j) = S_e(q,j)\|\alpha\|_p \left(\frac{1-2^{-(\bar{j}-j+1)\eta(p)}}{1-2^{-\eta(p)}} \right)^{q/p}. \quad (33)$$

D. Proof of Proposition 3

Let $n = q/p \in \mathbb{N}$, and let $l = j' - j$ and $m = \bar{j} - j$. The expected p-leader structure function is $\mathbb{E}\left[S_{\breve{\ell}^{(p)}}(q,j)\right] = \mathbb{E}\left[\left(\breve{\ell}_\lambda^{(p)}\right)^q\right]$. Further,

$$\mathbb{E}\left[\left(\breve{\ell}_\lambda^{(p)}\right)^q\right] = \mathbb{E}\left[\left(\sum_{l=0}^{m}\sum_{k=1}^{2^l} e_{j+l,k}^p 2^{-l}\right)^n\right] \quad (34)$$

$$= \mathbb{E}\left[\left(\sum_{l=0}^{m} \tilde{S}_\lambda(p,l)\right)^n\right], \quad (35)$$

where $\tilde{S}_\lambda$ is the structure function of the RWS subtree rooted at coefficient e_λ. Construction of the RWS implies that

$$\mathbb{E}\left[\tilde{S}_\lambda(p,l)\right] = \mathbb{E}\left[e_{j+l,\cdot}^p\right] = \mathbb{E}\left[\{W^p\}^{(j+l)}\right] = 2^{-(j+l)\eta(p)}. \quad (36)$$

Lower bound: Since the function $x \mapsto x^n$ is convex for $n \in \mathbb{N}^+$, we use Jensen's inequality to get

$$\mathbb{E}\left[\left(\sum_{l=0}^{m} \tilde{S}_\lambda(p,l)\right)^n\right] \geq \left(\sum_{l=0}^{m} \mathbb{E}\left[\tilde{S}_\lambda(p,l)\right]\right)^n \quad (37)$$

$$\geq \left(\sum_{l=0}^{m} 2^{-(j+l)\eta(p)}\right)^n \quad (38)$$

$$\geq 2^{-jn\eta(p)}\gamma^n(j,\eta(p)), \quad (39)$$

which proves the lower bound in (17).

Upper bound: First we use the multinomial theorem on (35) and the fact that $\tilde{S}_\lambda(p,l)$ are independent wrt l:

$$\mathbb{E}\left[\left(\sum_{l=0}^{m} \tilde{S}_\lambda(p,l)\right)^n\right] = \sum_{\sum r_l = n} \binom{n}{r_0,\ldots,r_m} \prod_{l=0}^{m} \mathbb{E}\left[\tilde{S}_\lambda^{r_l}(p,l)\right], \quad (40)$$

Since $r_l \in \mathbb{N}$ for all l, we use (36) and the multinomial theorem again, which reads for $r \in \mathbb{N}$:

$$\mathbb{E}\left[\tilde{S}_\lambda^r(p,l)\right] = 2^{-rl} \sum_{\sum s_k = r} \binom{r}{s_1,\ldots,s_{2^l}} \prod_{k=1}^{2^l} 2^{-(j+l)\eta(p\,s_k)}, \quad (41)$$

where we have used the independence of $e_{j+l,k}$ and (36). Since $s_k \in \mathbb{N}$ for all k, η is concave and $\eta(0) = 0$ we have:

$$\eta(p\,s_k) \geq \frac{s_k}{r}\eta(rp). \quad (42)$$

Using (42) in (41) yields

$$\mathbb{E}\left[\tilde{S}_\lambda^r(p,l)\right] \leq 2^{-(j+l)\eta(rp)}. \quad (43)$$

Finally, (43) in (40) produces

$$\mathbb{E}\left[\left(\sum_{l=0}^{m} \tilde{S}_\lambda(p,l)\right)^n\right] \leq \mathbb{E}[e_\lambda^q]\,\gamma^n\left(j, \frac{\eta(np)}{n}\right), \quad (44)$$

which proves the upper bound in (17).

E. Proof of Consequence 1

Let $r \in \mathbb{R}^+$ and $n \in \mathbb{N}^+$. Consider the polynomial interpolation

$$S_{\breve{\ell}^{(p)}}(rp,j) = \sum_{n=0}^{N} S_{\breve{\ell}^{(p)}}(np,j)h_n(x), \quad (45)$$

where the $h_n(x)$ are the Lagrange basis polynomials. Under the smoothness assumption (i.e. $\|\partial^{N+1} S_{\ell^{(p)}}(rp,j)/\partial r^{N+1}\|_\infty$ is small enough) we can ignore the interpolation error. Use of the lower bound in (17) in (45) yields

$$S_{\breve{\ell}^{(p)}}(rp,j) \geq \sum_{n=0}^{N} S_e(np,j)\,\gamma^{np}(j,\eta(p))\; b_S(n,p,j)\,h_n(x),$$

$$\geq S_e(rp,j)\,\gamma^{rp}(j,\eta(p))\; b_S(r,p,j), \quad (46)$$

which proves the lower bound. The proof of the converse statement is similar.

F. Proof of Propositions 4 and 5

Proposition 4 follows from (34), with $n = 1$. We now prove Proposition 5. Expanding (34), with $n = 2$, the expected value of restricted p-leaders is given by

$$\mathbb{E}\left[(\breve{\ell}_\lambda^{(p)})^{2p}\right] = \mathbb{E}\left[e_\lambda^{2p}\right] \sum_{l_1=0}^{\bar{j}-j}\sum_{l_2=0}^{\bar{j}-j}\sum_{k_1=1}^{2^{l_1}}\sum_{k_2=1}^{2^{l_2}} \mathbb{E}\left[e_{l_1,k_1}^p e_{l_2,k_2}^p 2^{-l_1-l_2}\right]. \quad (47)$$

Since wavelet coefficients of RWC are not independent, we cannot factorize the expected value $\mathbb{E}[e_{\lambda_1} e_{\lambda_2}]$.

Let $h : \mathbb{Z}^4 \to [0, \min(l_1,l_2)]$ such that $h(l_1,l_2,k_1,k_2)$ is the scale of the lowest common ancestor between coefficients e_{l_1,k_1} and e_{l_2,k_2}. Then, as in [25], we can write $e_{l_1,k_1} = W_1 \ldots W_{h(l_1,l_2,k_1,k_2)} W^{(1)}_{h(l_1,l_2,k_1,k_2)+1} \ldots W^{(1)}_{l_1}$ and $e_{l_2,k_2} = W_1 \ldots W_{h(l_1,l_2,k_1,k_2)} W^{(2)}_{h(l_1,l_2,k_1,k_2)+1} \ldots W^{(2)}_{l_2}$ where W_i, $W_i^{(1)}$ and $W_i^{(2)}$ are iid random variables. Note that the first $h(l_1,l_2,k_1,k_2)$ multipliers are the same for both coefficients. Therefore

$$\mathbb{E}\left[e_{l_1,k_1}^p e_{l_2,k_2}^p\right] = \mathbb{E}\left[W^{2p}\right]^{h(l_1,l_2,k_1,k_2)} \times \mathbb{E}[W^p]^{l_1+l_2-2h(l_1,l_2,k_1,k_2)}.$$

Using this in (47), and reordering we have:

$$\mathbb{E}\left[(\breve{\ell}_{\lambda}^{(p)})^{2p}\right] = 2^{-j\eta(2p)}\left(\sum_{l_1=0}^{\bar{j}-j}\sum_{l_2=0}^{\bar{j}-j} 2^{-l_1-l_2}\,\mathbb{E}[W^p]^{l_1+l_2}\cdot \right.$$
$$\left.\cdot \sum_{l=0}^{\min(l_1,l_2)} N(l_1,l_2,l)\frac{\mathbb{E}\left[W^{2p}\right]^l}{\mathbb{E}[W^p]^{2l}}\right). \quad (48)$$

where the function N represents the level sets of h:

$$N(l_1,l_2,l) = \#\left\{(k_1,k_2)\ :\ h(l_1,l_2,k_1,k_2) = l\right\}. \quad (49)$$

To compute N, let $l \leq \min(l_1,l_2)$. Consider the subtree rooted at coefficient $e_{l,k}$ (note that there are 2^l such subtrees): it has 2^{l_2-l} children at scale l_2 and 2^{l_1-l} children at scale l_1. Then, the total number of pairs $(e_{l_1,k_1}, e_{l_2,k_2})$ which have $e_{l,k}$ as a parent is $2^{l_1-l}2^{l_2-l}$. Since there are 2^l possible choices for the root $e_{l,k}$ we have:

$$N(l_1,l_2,l) = 2^{l_1-l}2^{l_2-l}2^l = 2^{l_1+l_2-l} \quad (50)$$

Using (50) in (48), splitting the sum over l and summing the geometric sums, (21) follows.

REFERENCES

[1] R. Leonarduzzi, G. Alzamendi, G. Schlotthauer, and M. Torres, "Wavelet leader multifractal analysis of period and amplitude sequences from sustained vowels," *Speech Commun.*, vol. 72, pp. 1–12, 2015.

[2] A. Arneodo, C. Vaillant, B. Audit, F. Argoul, Y. d'Aubenton Carafa, and C. Thermes, "Multi-scale coding of genomic information: From DNA sequence to genome structure and function," *Phys. Rep.*, vol. 498, no. 2, pp. 45–188, 2011.

[3] B. B. Mandelbrot, "A multifractal walk down Wall Street," *Sci. Amer.*, vol. 280, no. 2, pp. 70–73, 1999.

[4] L. Telesca and M. Lovallo, "Analysis of the time dynamics in wind records by means of multifractal detrended fluctuation analysis and the Fisher–Shannon information plane," *J. Statist. Mech., Theory Experiment*, vol. 2011, no. 07, 2011, Art. no. P07001.

[5] Y. Tessier, S. Lovejoy, and D. Schertzer, "Universal multifractals: Theory and observations for rain and clouds," *J. Appl. Meteorol.*, vol. 32, no. 2, pp. 223–250, 1993.

[6] P. Abry, S. Jaffard, and H. Wendt, "When Van Gogh meets Mandelbrot: Multifractal classification of painting's texture," *Signal Process.*, vol. 93, no. 3, pp. 554–572, 2013.

[7] S. Jaffard, "Wavelet techniques in multifractal analysis," in *Fractal Geometry and Applications: A Jubilee of Benoît Mandelbrot*, vol. 72, M. Lapidus and M. van Frankenhuijsen, Eds. Providence, RI, USA: AMS, 2004, pp. 91–152.

[8] J. W. Kantelhardt, S. A. Zschiegner, E. Koscielny-Bunde, S. Havlin, A. Bunde, and H. E. Stanley, "Multifractal detrended fluctuation analysis of nonstationary time series," *Physica A*, vol. 316, no. 1, pp. 87–114, 2002.

[9] J. F. Muzy, E. Bacry, and A. Arneodo, "Multifractal formalism for fractal signals: The structure-function approach versus the wavelet-transform modulus-maxima method," *Phys. Rev. E*, vol. 47, no. 2, pp. 875–884, 1993.

[10] S. Jaffard *et al.*, "p-exponent and p-leaders, Part I: Negative pointwise regularity," *Physica A*, vol. 448, pp. 300–318, 2016.

[11] R. Leonarduzzi *et al.*, "p-exponent and p-leaders, Part II: Multifractal analysis. Relations to detrended fluctuation analysis," *Physica A*, vol. 448, pp. 319–339, 2016.

[12] S. Jaffard, P. Abry, C. Melot, R. Leonarduzzi, and H. Wendt, "Multifractal analysis based on p-exponents and lacunarity exponents," in *Fractal Geometry and Stochastics V* (Progress in Probability), vol. 70, C. Bandt, K. Falconer, and M. Zahle, Eds. Basel, Switzerland: Birkhäuser, 2015, pp. 279–313.

[13] P. Abry, S. Jaffard, R. Leonarduzzi, C. Melot, and H. Wendt, "New exponents for pointwise singularities classification," in *Proc. Fractals Related Fields III*, S. Seuret and J. Barral, Eds., Sep. 19–26, 2015, Porquerolles, France, 2017, to be published.

[14] H. Wendt, P. Abry, and S. Jaffard, "Bootstrap for empirical multifractal analysis," *IEEE Signal Process. Mag.*, vol. 24, no. 4, pp. 38–48, Jul. 2007.

[15] H. Wendt, S. G. Roux, S. Jaffard, and P. Abry, "Wavelet leaders and bootstrap for multifractal analysis of images," *Signal Process.*, vol. 89, no. 6, pp. 1100–1114, 2009.

[16] P. Abry and P. Flandrin, "On the initialization of the discrete wavelet transform algorithm," *IEEE Signal Process. Lett.*, vol. 1, no. 2, pp. 32–34, Feb. 1994.

[17] D. Veitch, M. S. Taqqu, and P. Abry, "Meaningful MRA initialization for discrete time series," *Signal Process.*, vol. 80, no. 9, pp. 1971–1983, Sep. 2000.

[18] A. P. Calderon and A. Zygmund, "Local properties of solutions of elliptic partial differential equations," *Studia Mathematica*, vol. 20, pp. 171–223, 1961.

[19] S. Jaffard and C. Melot, "Wavelet analysis of fractal boundaries," *Commun. Math. Phys.*, vol. 258, no. 3, pp. 513–565, 2005.

[20] S. Mallat, *A Wavelet Tour of Signal Processing*. San Diego, CA, USA: Academic, 1998.

[21] B. Castaing, Y. Gagne, and M. Marchand, "Log-similarity for turbulent flows," *Physica D*, vol. 68, nos. 3/4, pp. 387–400, 1993.

[22] S. Jaffard, P. Abry, and S. G. Roux, "Function spaces vs. scaling functions: Tools for image classification," in *Mathematical Image Processing* (Springer Proceedings in Mathematics), vol. 5, M. Bergounioux, Ed. New York, NY, USA: Springer, 2011, pp. 1–39.

[23] N. Decoster, S. Roux, and A. Arneodo, "A wavelet-based method for multifractal image analysis. ii. Applications to synthetic multifractal rough surfaces," *Eur. Phys. J. B-Condensed Matter Complex Syst.*, vol. 15, no. 4, pp. 739–764, 2000.

[24] J. M. Aubry and S. Jaffard, "Random wavelet series," *Commun. Math. Phys.*, vol. 227, no. 3, pp. 483–514, 2002.

[25] A. Arneodo, E. Bacry, and J. F. Muzy, "Random cascades on wavelet dyadic trees," *J. Math. Phys.*, vol. 39, no. 8, pp. 4142–4164, Aug. 1998.

[26] B. Mandelbrot and J. Van Ness, "Fractional brownian motions, fractional noises and applications," *SIAM Rev.*, vol. 10, no. 4, pp. 422–437, Oct. 1968.

[27] G. Samorodnitsky and M. Taqqu, *Stable Non-Gaussian Random Processes*. New York, NY, USA: Chapman & Hall, 1994.

[28] E. Bacry, J. Delour, and J.-F. Muzy, "Multifractal random walk," *Phys. Rev. E*, vol. 64, 2001, Art. no. 026103.

[29] L. Chevillard, R. Robert, and V. Vargas, "A stochastic representation of the local structure of turbulence," *Europhys. Lett.*, vol. 89, no. 5, 2010, Art. no. 54002.

[30] S. Jaffard, "The multifractal nature of Lévy processes," *Probab. Theory Related Fields*, vol. 114, pp. 207–227, 1999.

[31] R. Leonarduzzi, H. Wendt, S. Jaffard, and P. Abry, "Pitfall in multifractal analysis of negative regularity," in *Proc. GRETSI Symp. Signal Image Process.*, Lyon, France, Sep. 2015, pp. 1–4.

[32] A. L. Goldberger *et al.* "PhysioBank, PhysioToolkit, and PhysioNet: Components of a new research resource for complex physiologic signals," *Circulation*, vol. 101, no. 23, pp. e215–e220, 2000.

[33] J. Spilka, J. Frecon, R. Leonarduzzi, N. Pustelnik, P. Abry, and M. Doret, "Sparse support vector machine for intrapartum fetal heart rate classification," *IEEE J Biomed. Health Informat.*, preprint, DOI: 10.1109/JBHI.2016.2546312